THE JOURNAL OF BIOLOGICAL CHEMISTRY VOL. 286, NO. 5, pp. 3342–3350, February 4, 2011

The NPC Motif of Aquaporin-11, Unlike the NPA Motif of Known Aquaporins, Is Essential for Full Expression of Molecular Function*

Received for publication, September 1, 2010, and in revised form, November 25, 2010 Published, JBC Papers in Press, November 30, 2010, DOI 10.1074/jbc.M110.180968

Masahiro Ikeda[‡1], Ayaka Andoo[‡], Mariko Shimono[‡], Natsuko Takamatsu[‡], Asaka Taki[‡], Kanako Muta[‡], Wataru Matsushita[‡], Tamayo Uechi[§], Toshiyuki Matsuzaki[¶], Naoya Kenmochi[§], Kuniaki Takata[¶], Sei Sasaki[‖], Katsuaki Ito[‡], and Kenichi Ishibashi[**]

From the [‡]Department of Veterinary Pharmacology and [§]Frontier Science Research Center, University of Miyazaki, Miyazaki 889-2192, Japan, the [¶]Department of Anatomy and Cell Biology, Gunma University Graduate School of Medicine, Maebashi 371-8511, Japan, the [‖]Department of Nephrology, Tokyo Medical and Dental University, Tokyo 113-8519, Japan, and the [**]Department of Medical Physiology, Meiji Pharmaceutical University, Tokyo 204-8588, Japan

The recently identified molecule aquaporin-11 (AQP11) has a unique amino acid sequence pattern that includes an Asn-Pro-Cys (NPC) motif, corresponding to the N-terminal Asn-Pro-Ala (NPA) signature motif of conventional AQPs. In this study, we examined the effect of the mutation of the NPC motif on the subcellular localization, oligomerization, and water permeability of AQP11 in transfected mammalian cells. Furthermore, the effect was also assessed using zebrafish. Site-directed mutation at the NPC motif did not affect the subcellular localization of AQP11 but reduced its oligomerization. A cell swelling assay revealed that cells expressing AQP11 with a mutated NPC motif had significantly lower osmotic water permeability than cells expressing wild-type AQP11. Zebrafish deficient in endogenous AQP11 showed a deformity in the tail region at an early stage of development. This phenotype was dramatically rescued by injection of human wild-type AQP11 mRNA, whereas the effect of mRNA for AQP11 with a mutated NPC motif was less marked. Although the NPA motif is known to be important for formation of water-permeable pores by conventional AQPs, our observations suggest that the corresponding NPC motif of AQP11 is essential for full expression of molecular function.

The aquaporins (AQPs)[2] are a family of membrane water channel proteins found throughout the animal and plant kingdoms (1, 2). The AQPs characterized to date all exist as multisubunit oligomers (homotetrameric assemblies found in most AQPs), and this oligomerization is suggested to be important for their function (3, 4). Almost all AQPs have two highly conserved Asn-Pro-Ala (NPA) motifs in each subunit, and these represent the signature motifs of the AQPs (1, 2, 5). Structural analysis of AQP1, the first AQP molecule to be identified, has shown that these motifs reside on opposite sides of the AQP1 monomer and are important for water-selective pore formation (2, 3).

So far, sequence analysis has revealed 13 functionally and phylogenetically distinct members of the AQP family in mammals, comprising three subgroups: the water-selective AQPs (AQP0, AQP1, AQP2, AQP4, AQP5, AQP6, and AQP8), aquaglyceroporins (AQP3, AQP7, AQP9, and AQP10), and a recently proposed third group (AQP11 and AQP12) (1, 2, 5). The water-selective AQPs are all permeated by water molecules, but AQP6 is additionally permeable to a wide range of anions, and AQP8 can facilitate the movement of ammonia and hydrogen peroxide across the plasma membrane (1, 5). The aquaglyceroporins are characterized by permeability to water and neutral solutes, in particular glycerol (1, 5). Compared with the water-selective AQPs and aquaglyceroporins, the sequence alignments of mammalian AQPs indicate that AQP11 and AQP12 are the most distantly related paralogs. At the amino acid level, AQP11 is ~10% identical and AQP12 is ~25% identical to the previously characterized members (6–8). AQP11 is most similar to AQP12 (with ~23% identity). When compared with the signature motifs of other mammalian AQPs, the C-terminal NPA motif is conserved in both AQP11 and AQP12, but the N-terminal NPA motif is deviated to an Asn-Pro-Cys (NPC) motif for AQP11 and to an Asn-Pro-Thr (NPT) motif for AQP12. Because of their low homologies and deviation from the N-terminal NPA motif, it is difficult to include both AQP11 and AQP12 in the water-selective AQP or aquaglyceroporin subgroup. Furthermore, similar orthologs have been found in nematodes, fruit fly, fish, frog, and chicken (5). Therefore, it has been proposed that AQP11 and AQP12 together with similar orthologs should be classified into a third AQP group (2, 5).

Of the AQPs thought to belong to the third group, mammalian AQP11 is the most characterized. Immunohistochemical studies have shown that AQP11 may work as a sort of intracellular AQP molecule in certain tissues, such as the kidney and brain (6, 7). AQP11-null mice die in the neonatal period due to renal failure with progressive renal cyst formation, suggesting the importance of AQP11 in mammalian kidney development (6, 9). Recently, it was reported that AQP11 also

* This work was supported by Japan Society for the Promotion of Science KAKENHI Grants 17580259 (to M. I.) and 19580342 (to M. I.).

[1] To whom correspondence should be addressed: Dept. of Veterinary Pharmacology, Faculty of Agriculture, University of Miyazaki, Gakuenkibanadai-Nishi 1-1, Miyazaki 889-2192, Japan. Tel.: 81-985-58-7268; Fax: 81-985-58-7268; E-mail: a0d302u@cc.miyazaki-u.ac.jp.

[2] The abbreviations used are: AQP, aquaporin; ER, endoplasmic reticulum; DSP, dithiobis (succinimidyl propionate); MO, morpholino antisense oligonucleotide.

played significant roles in mammalian spermatogenesis and salivary gland development (10, 11). Thus AQP11 is thought to be an important intracellular molecule for the development of certain organs. For the channel properties, no data for the third AQP group other than AQP11 have yet been reported. A reconstruction vesicle study has revealed that AQP11 is permeable to the water molecule, suggesting that AQP11 is a water channel and that the NPC motif of AQP11 and the corresponding N-terminal NPA motif found in water-selective AQPs are exchangeable (12). However, the role of its divergent motif of AQP11 is still unclear.

In order to gain insight into the nature of the divergent motif of AQP11, we examined its role in the subcellular localization, oligomerization, and water permeability of the molecule in transfected mammalian cells. Furthermore the role was also evaluated using zebrafish. Our data indicate that the NPC motif of AQP11, unlike the NPA motif of known AQPs, is essential for full functional expression of the molecule.

EXPERIMENTAL PROCEDURES

Plasmid Construction, Cell Culture, Transfection, and Confocal Microscopy—The Myc-, GFP-, or V5-tagged AQP11 construct was made by in-frame subcloning of mouse *AQP11* cDNA into the pCMV-Myc (BD Biosciences Clontech), pEGFP-C1 (BD Biosciences Clontech), pcDNA-DEST47 (Invitrogen), pcDNA3.1/nV5-DEST (Invitrogen), or pcDNA-DEST40 (Invitrogen) vector. The pDsRed2-ER vector (BD Biosciences Clontech) was used for fluorescent labeling of the ER. The mutations of the constructs were introduced by site-directed mutagenesis (Stratagene).

CHO-K1 cells (obtained from ATCC, catalog no. CCL-61) were transfected at 50–60% confluence using Lipofectamine 2000 (Invitrogen) as described previously (13). Cultured cells on glass coverslips in 35-mm dishes were observed 24 h post-transfection using an FV-300 confocal microscope (Olympus, Japan).

Surface Biotinylation—After transfection, CHO-K1 cells were biotinylated in 1 mg/ml sulfo-NHS-SS-biotin (Pierce) at 4 °C for 10–15 min as described previously (14). After washing, the cells were lysed in lysis buffer (25 mM Tris, pH 7.4, 150 mM NaCl, 2 mM EDTA, 2% Nonidet P-40, Complete protease inhibitor mixture) for 30 min at 4 °C, and the cell lysate was then centrifuged at 12,000 × *g* for 10 min. The resulting supernatant was precipitated with immobilized NeutrAvidin beads (Pierce).

Immunoprecipitation—Transfected CHO-K1 cells were lysed, and the lysate was incubated with anti-Myc (Sigma) or anti-V5-agarose beads (Bethyl Laboratories, Montgomery, TX). After washing, the beads were mixed with 4× Laemmli sample buffer supplemented with 0.2 M DTT at 37 °C for 60 min.

Cross-linking Experiments—Transfected CHO-K1 cells were lysed in lysis buffer (25 mM Tris, pH 7.4, 150 mM NaCl, 2 mM EDTA, 4% sodium deoxycholate, Complete protease inhibitor mixture), and the lysate was incubated with 150 μM dithiobis(succinimidyl propionate) (DSP) at room temperature (25 °C) for 30 min. Ethanolamine (final concentration 50 mM) was then added to the lysate, and the lysate was mixed with 2× Laemmli sample buffer (62.5 mM Tris, pH 6.8, 25% glycerol, 2% SDS, 0.01% bromphenol blue) supplemented with or without 0.1 M DTT at 37 °C for 20 min.

For cross-linking with paraformaldehyde, cells were incubated with PBS containing 4% paraformaldehyde at room temperature for 15 min. After washing, the cells were lysed in lysis buffer (25 mM Tris, pH 7.4, 150 mM NaCl, 2 mM EDTA, 1.5% Nonidet P-40, Complete protease inhibitor mixture), and the lysate was then mixed with 2× Laemmli sample buffer supplemented with 0.1 M DTT at 37 °C for 20 min.

Measurement of Osmotic Water Permeability (Pf)—One day after transfection, CHO-K1 cells were treated with trypsin-EDTA for 15 s to create a round cell shape, allowing easy calculation of cell volume. The cells were then washed and immersed in an extracellular solution containing 150 mM NaCl, 1 mM $MgCl_2$, 1 mM $CaCl_2$, and 10 mM Hepes (pH 7.4 with Tris). The cells expressing GFP were identified under a laser-scanning confocal microscope (FV300). Osmotic swelling was induced at 25 °C by puff application of a hypotonic solution made by dilution of extracellular solution 1:1 in MilliQ water. The puff application was performed using a nearby pipette of 30–35 μm diameter. An image frame of the cell was recorded every 1.12 s using a time lapse image capture system attached to the microscope. *Pf* was calculated from osmotic swelling data obtained between 1.12 and 15.68 s using the formula,

$$Pf = (V_0 \times d(V/V_0)/dt)/(S \times V_w \times (osm_{in} - osm_{out})) \quad \text{(Eq. 1)}$$

where V_0 and S are the initial cell volume and surface area, respectively, $d(V/V_0)/dt$ is the slope of linear fit for the plot of cell volume *versus* time between 1.12 and 15.68 s during osmotic swelling, and $V_w \times (osm_{in} - osm_{out})$ is the osmolality gradient.

Zebrafish Experiments—Zebrafish experiments were performed as described previously (15). In brief, morpholino antisense oligonucleotides (MOs) were obtained from Gene Tools, LLC (Philomath, OR). The sequences of the MOs used in this study were as follows (see Fig. 6*A*): MO2, 5′-CAAAAACTAATCCAGACAGGCAACT-3′; MO3, 5′-AAACGCAGTGATTCTACAAACCCGC-3′; MO4, 5′-TGTCCACCTTTACAAAACACAACAC-3′; MO5, 5′-TGTTGTAATTCTGCTCACCTAGTAT-3′; control MO, 5-bp mismatched MO5, 5′-TcTTcTAATTCTcCTCAgCTAcTAT-3′ (lowercase letters indicate mismatched bases in MO5). A total amount of 2 or 4 ng of each MO was injected into one-cell-stage embryos. *In vitro* transcribed 5′-capped mRNAs encoding GFP, human AQP11 (hAQP11), and hAQP11 with Cys^{101} mutated to Ala (hAQP11-C101A) were synthesized using a mMessage mMachine® T7 kit (Ambion), and 80–150 pg of capped mRNA was injected. For the RT-PCR, total RNA was isolated from 24-h postfertilization larvae using an RNeasy® Protect minikit (Qiagen, MD). The zebrafish AQP11-specific primers used were as follows: forward, TTCATCATCTCGGTGGTTCA; reverse, TCATCTTTTTCTTCTTGAGTCCA.

Western Blot Analysis and Chemicals—After separation by SDS-PAGE, the protein was transferred to a polyvinylidene difluoride membrane, and the protein on the membrane associated with antibodies was detected by a SuperSignal® chemi-

luminescence detection system (Pierce). Antibodies used in this study were anti-Myc antibody (BD Biosciences Clontech), anti-V5 antibody (Invitrogen), and anti-GFP antibody (Molecular Probes). All other chemicals and reagents were from Sigma or Wako Pure Chemicals (Japan).

RESULTS

Subcellular Localization of AQP11-C101A Mutant—It has been reported that AQP11 is localized at the endoplasmic reticulum (ER) membrane (6). We investigated whether the introduction of a mutation at Cys^{101}, replacing it with Ala, affected the subcellular localization of AQP11. CHO-K1 cells were transfected with C-terminal GFP-tagged human AQP1 (hAQP1-GFP), N-terminal GFP-tagged mouse AQP11 (GFP-AQP11), C-terminal GFP-tagged AQP11 (AQP11-GFP), and GFP-AQP11-C101A expression plasmids together with a plasmid encoding an ER marker protein. Twenty-four hours after transfection, the cells were observed with a confocal microscope. AQP1-GFP was clearly localized in the cytoplasm as well as at the plasma membrane (Fig. 1*A*). In contrast, the localizations of GFP-AQP11 (Fig. 1*B*) and AQP11-GFP (data not shown) virtually overlapped that of the ER marker. These data confirmed a previous report that AQP11 is localized mainly in the ER (6). Moreover, even when a larger protein molecule, such as GFP, was used to tag the N or C terminus of AQP11, its subcellular localization was unchanged. As shown in Fig. 1*C*, GFP-AQP11-C101A was clearly localized in the ER, indicating that the NPC motif might not be related to the intracellular localization of AQP11.

Cell surface expression levels of Myc-AQP11 and Myc-AQP11-C101A were further assessed by biotinylation experiments. The abundance of the biotinylated protein did not differ between Myc-AQP11 and Myc-AQP11-C101A (Fig. 1, *D* and *E*), confirming the intracellular localization of GFP-AQP11-C101A revealed by fluorescence microscopy. In addition, the presence of a significant amount of cell surface Myc-AQP11 and Myc-AQP11-C101A was noteworthy.

Oligomerization State of AQP11—So far, biochemical and structural analyses have revealed that the water-selective AQPs have a tetrameric structure (2, 3). A sucrose density gradient ultracentrifugation experiment by Gorelick *et al.* (7) has also shown that AQP11 sediments in fractions similar, but not identical, to those of AQP4, which is known to form tetramers (16), suggesting that AQP11 may also be capable of tetramer formation. We therefore examined the oligomerization state of AQP11 using techniques other than sucrose density gradient ultracentrifugation, such as co-immunoprecipitation and chemical cross-linking. CHO-K1 cells were transfected with either or both of the expression plasmids Myc-AQP11 and AQP11-V5, and 24 h later, the cellular proteins were precipitated using anti-Myc- or anti-V5-agarose beads. The precipitates were then subjected to Western blotting analysis using anti-Myc or anti-V5 antibody. As shown in Fig. 2*A*, after precipitation with anti-Myc-agarose beads, only the precipitates from cells expressing both Myc-AQP11 and AQP11-V5 were reactive with the anti-V5 antibody. Also, after precipitation with anti-V5-agarose beads, only the precipitates from cells expressing both proteins were reactive

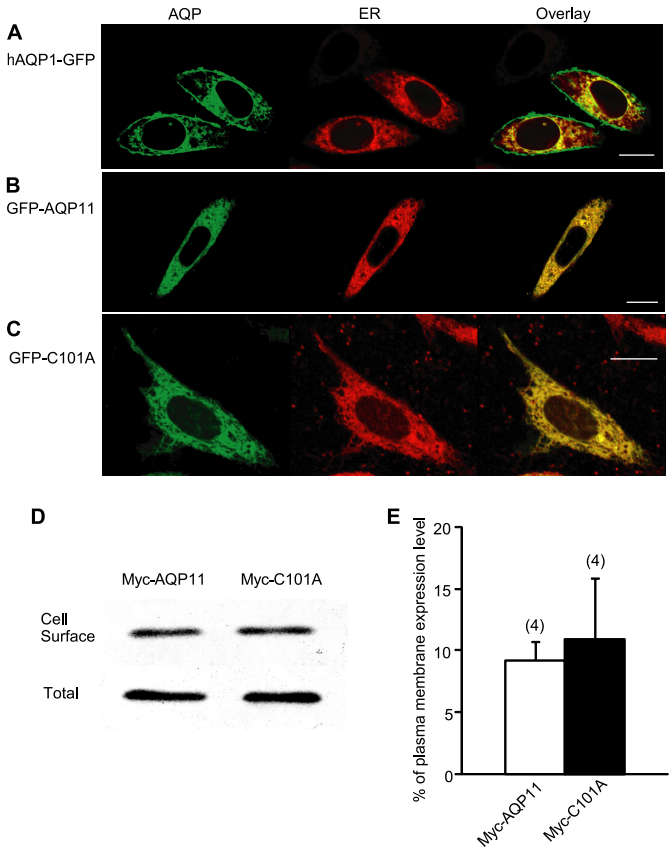

FIGURE 1. **Subcellular localization of AQP11 mutant.** *A–C*, subcellular localizations of hAQP1-GFP, GFP-AQP11, and GFP-AQP11-C101A (*GFP-C101A*) were evaluated by fluorescence microscopy. CHO-K1 cells were co-transfected with hAQP1-GFP (*A*), GFP-AQP11 (*B*), or GFP-C101A (*C*) expression plasmid and a plasmid encoding an ER marker protein (pDsRed2-ER). The cells were observed with a confocal microscope 24 h post-transfection. *Green* and *red* indicate AQPs and ER marker proteins, respectively. *Scale bars*, 10 μm. Experiments were repeated more than three times with similar results. *D*, cell surface expression levels of Myc-AQP11 and Myc-AQP11-C101A (Myc-C101A) were assessed by a biotinylation experiment. CHO-K1 cells were transfected with Myc-AQP11 or Myc-C101A expression plasmid, and 24 h post-transfection, the cell surface proteins were labeled with membrane-impermeable biotin. The biotin-labeled proteins were precipitated by NeutrAvidin beads. The biotin-labeled cell surface proteins as well as the total cell lysates were analyzed by Western blotting using anti-Myc antibody. *E*, densitometric analysis of biotinylated Myc-tagged proteins is summarized. The ratio of biotinylated to total Myc-tagged proteins was taken as an index of the cell surface expression level. Values are presented as mean ± S.E. (*error bars*). The numbers of experiments are given in *parentheses*. No statistical significant difference was found between the two groups (Student's *t* test).

with the anti-Myc antibody. These results clearly indicate that Myc-AQP11 interacts with AQP11-V5.

Because a chemical cross-linking experiment with DSP has shown that AQP4 has an oligomeric structure (16), DSP was used to further investigate the oligomeric structure of AQP11-V5. Without DSP treatment, only a 25 kDa protein band was observed (Fig. 2*B*). However, after treatment of cell lysate with DSP, Western blotting analysis yielded a band at ~50 kDa in addition to a band at ~25 kDa. This 50 kDa protein band disappeared when the cell lysate was further incubated with DTT, a strong reducing agent. Therefore, the 50 kDa band was likely to be dimerized AQP11. In some experiments, we observed a band at ~75 kDa, apparently corresponding to trimeric AQP11 (data not shown).

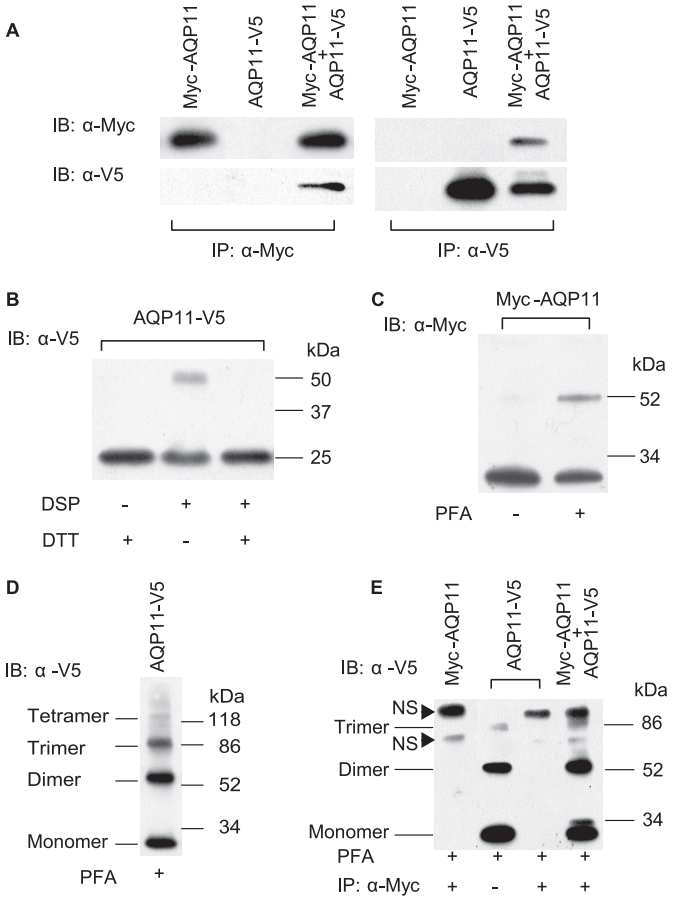

FIGURE 2. **Oligomerization of AQP11.** *A*, oligomerization between Myc-AQP11 and AQP11-V5 was assessed by a co-immunoprecipitation experiment. Twenty-four hours post-transfection, the cellular proteins were precipitated by anti-Myc-agarose (*IP*: α-*Myc*) or anti-V5-agarose beads (*IP*: α-*V5*). The precipitates were then analyzed by Western blotting using anti-Myc (*IB*: α-*Myc*) or anti-V5 antibody (*IB*: α-*V5*). Experiments were repeated three times with similar results. *B* and *C*, oligomerization state of AQP11-V5 was evaluated using a chemical cross-linker, DSP (*B*) or paraformaldehyde (*PFA*) (*C*). The cellular lysates from cells expressing AQP11-V5 or Myc-AQP11 were treated with DSP or PFA and then analyzed by Western blotting. Experiments were repeated three times for *B* and six times for *C* with similar results. *D*, a typical example of tetramerization of AQP11-V5 after treatment of cells expressing AQP11-V5 with paraformaldehyde. Experiments were repeated four times with similar results. *E*, oligomerization between Myc-AQP11 and AQP11-V5 after treatment with paraformaldehyde was assessed by a co-immunoprecipitation experiment. Cells were transfected with Myc-AQP11, AQP11-V5, or both expression plasmids. *NS* indicates non-specific band. The *second lane* was loaded with lysate from cells expressing only AQP11-V5. Experiments were repeated twice with similar results.

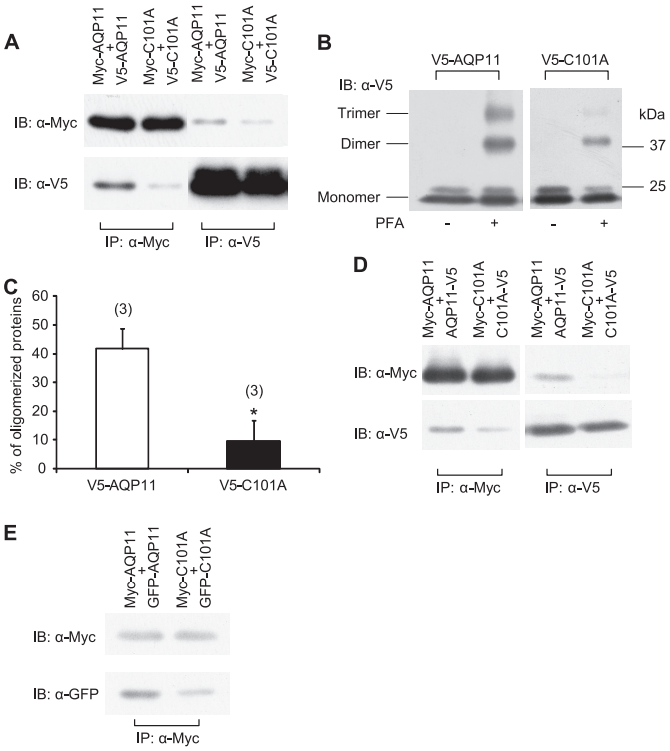

FIGURE 3. **Oligomerization of the AQP11-C101A mutant.** *A*, oligomerization between Myc-AQP11 and V5-AQP11 or Myc-AQP11-C101A (Myc-C101A) and V5-AQP11-C101A (V5-C101A) was assessed by a co-immunoprecipitation experiment. Experiments were repeated four times, and similar results were obtained. *B*, the oligomerization state of V5-C101A was evaluated using a chemical cross-linker, paraformaldehyde (*PFA*). Experiments were repeated three times. *C*, densitometric analysis of oligomerized proteins in *B* is summarized. The ratio of oligomerized proteins (more than dimer) to total proteins (monomer plus oligomerized proteins) was taken as an index of the oligomerization level. Values are presented as mean ± S.E. The numbers of experiments are given in *parentheses*. *, $p < 0.05$ *versus* V5-AQP11. Statistical significance was evaluated by Student's *t* test. *D* and *E*, oligomerization between Myc-C101A and AQP11-V5-C101A (C101A-V5) or GFP-AQP11-C101A (GFP-C101A) was assessed by a co-immunoprecipitation experiment. *IP*, immunoprecipitation; *IB*, immunoblot.

Paraformaldehyde, a fixative, has been reported to be a useful cross-linker for detection of the oligomeric structure of membrane proteins (17). We therefore used paraformaldehyde as another cross-linker to evaluate the oligomeric structure of AQP11. After the fixation of cells expressing Myc-AQP11, cellular proteins were prepared and analyzed by Western blotting. Fig. 2*C* shows a representative result. As observed, paraformaldehyde was able to produce a band at ~50 kDa in addition to a band at ~25 kDa. In some cases with paraformaldehyde, we observed bands at ~75 and 120 kDa, which corresponded to the trimeric and tetrameric structures of AQP11 as shown with AQP11-V5 (Fig. 2*D*). These results were very similar to those obtained with DSP. However, because use of paraformaldehyde is a first approach to study the oligomerization of AQP family proteins, we needed to check the legitimacy of this approach. Therefore, we performed the co-immunoprecipitation combined with paraformaldehyde fixation. CHO-K1 cells were transfected with either or both of the expression plasmids Myc-AQP11 and AQP11-V5, and 24 h after transfection, lysates prepared from the cells fixed with paraformaldehyde were precipitated using anti-Myc-agarose beads. The precipitates were then evaluated by Western blotting analysis using anti-V5 antibody. As shown in Fig. 2*E*, only the precipitates from cells expressing both Myc-AQP11 and AQP11-V5 produced bands corresponding to monomeric, dimeric, and trimeric AQP11. These data clearly indicate that paraformaldehyde cross-links the AQP11 subunits and produces visible oligomerized bands. Taken together, these results indicated that AQP11 exists as a multimerized protein, most likely a tetramer, as is the case for AQP1 and other AQPs (2, 3, 16).

Oligomerization State of AQP11 Mutants—Next, we examined the oligomerization state of the AQP11-C101A mutant. As shown in Fig. 3*A*, after precipitation with anti-Myc-agarose beads, the abundance of protein detected by the anti-V5 antibody was lower in cells co-expressing Myc- and V5-

AQP11-C101A in comparison with the wild-type form. Reciprocally, after precipitation with anti-V5-agarose beads, the precipitation of Myc-AQP11-C101A was reduced. On the other hand, the expression levels of V5- or Myc-tagged proteins in the two groups were quite similar. These results clearly indicate that C101A mutation in the NPC motif reduces the oligomerization of AQP11.

We also examined the oligomerization state of AQP11-C101A using cross-linkers. Chemical cross-linking with DSP (data not shown) or paraformaldehyde (Fig. 3, *B* and *C*) resulted in less multimer formation by V5-AQP11-C101A, compared with the wild-type form.

Furthermore, we evaluated the oligomerization between Myc-AQP11-C101A and AQP11-V5-C101A or Myc-AQP11-C101A and GFP-AQP11-C101A in a co-immunoprecipitation experiment. As shown in Fig. 3, *D* and *E*, even when we used different tags, reduced oligomer formation of AQP11-C101A was observed.

Hetero-oligomerization of AQP11 Mutants with the Wild-type Form—We examined the extent of oligomerization between the wild-type form and AQP11-C101A. The precipitate obtained with anti-Myc-agarose beads from cells co-expressing AQP11-V5 and Myc-AQP11-C101A reacted weakly with anti-V5 antibody (*lane 4* of the *lower panel* in Fig. 4*A*), compared with that from cells co-expressing AQP11-V5 and Myc-AQP11 (*lane 2*). On the other hand, the expression levels of V5- or Myc-tagged proteins in the two groups were quite similar, as shown in the lanes that were loaded with lysates. These results indicate that the C101A mutant forms oligomers poorly with wild-type AQP11.

Finally, we examined the effect of mutations in and around the NPC motif on the degree of oligomerization between wild-type AQP11 and the mutants. As shown in Fig. 4*B*, the V5-AQP11-C101T and -N99D mutants formed oligomers poorly with wild-type AQP11. On the other hand, no reduction of oligomer formation by V5-AQP11-G102V with the wild-type form was observed. These findings again indicate the importance of the NPC motif in the oligomerization of AQP11.

Measurement of Pf—As mentioned earlier, cell surface biotinylation experiments with CHO-K1 cells expressing AQP11 revealed that AQP11 was expressed mainly in intracellular components. However, a significant amount of AQP11 was also detected at the plasma membrane (Fig. 1, *D* and *E*), thus possibly allowing measurement of the water permeability of AQP11 using a conventional cell swelling assay. We therefore measured the osmotic water permeability of cells expressing GFP-AQP11 using the method. As shown in Fig. 5*A*, treatment with a hypotonic solution caused swelling more rapidly in cells expressing GFP-AQP11 than in mock cells. The *Pf* values (Fig. 5*B*), shown as mean ± S.E., were 8.0 ± 0.7 cm/s × 10^{-4} ($n = 12$) for cells expressing GFP-AQP11 and 4.8 ± 0.8 cm/s × 10^{-4} ($n = 12$) for the mock cells.

Because it proved possible to measure the water permeability of AQP11 using this assay, we then used it to measure the osmotic water permeability of cells expressing GFP-AQP11-C101A. As shown in Fig. 5, *A* and *B*, cells expressing GFP-AQP11-C101A showed no significant water permeability

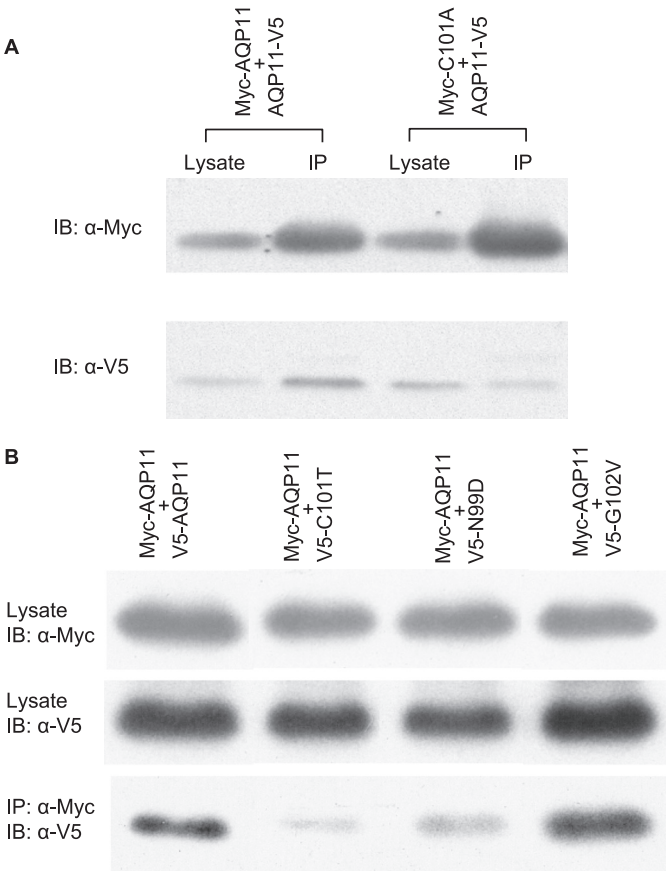

FIGURE 4. **Oligomerization between the wild-type form and its mutant protein.** *A*, oligomerization between AQP11-V5 and Myc-AQP11 or Myc-C101A was assessed by a co-immunoprecipitation experiment. Experiments were repeated twice with similar results. *B*, oligomerization between Myc-AQP11 and V5-AQP11, V5-AQP11-C101T (*V5-C101T*), AQP11-V5-N99D (*V5-N99D*), or AQP11-V5-G102V (*V5-G102V*) was assessed by a co-immunoprecipitation experiment. Experiments were repeated three times with similar results. *IP*, immunoprecipitation; *IB*, immunoblot.

(*Pf* = 3.8 ± 0.9 cm/s × 10^{-4}, $n = 12$), compared with that of mock cells. Because the plasma membrane expression level of AQP11-C101A was not significantly different from that of mock cells (Fig. 1*E*), these data indicate that the NPC motif of AQP11 plays an important role in the water permeability function of the molecule.

Effect of hAQP11-C101A Capped mRNA on the Phenotype of Zebrafish Deficient in Endogenous AQP11—It has been reported that, in zebrafish, disruption of endogenous AQP11 by MO results in body axis curvature of the morphants and that this phenotype was rescued by co-injecting hAQP11 mRNA (18). We therefore employed this system to evaluate the importance of Cys^{101} for the function of AQP11. Because the nucleotide sequence around the initiation codon of zebrafish *aqp11* was ambiguous in the NCBI and Ensembl databases (19), we originally designed four MOs that would be potentially capable of blocking sites involved in splicing the pre-mRNA of zebrafish *aqp11* and screened them. Among these four MOs (MO2–MO5), MO5 was found to be the most effective for splice inhibition, as judged by RT-PCR and sequence analysis, and also for inducing a higher number of morphants showing body axis curvature. Therefore, we used MO5 for further experiments.

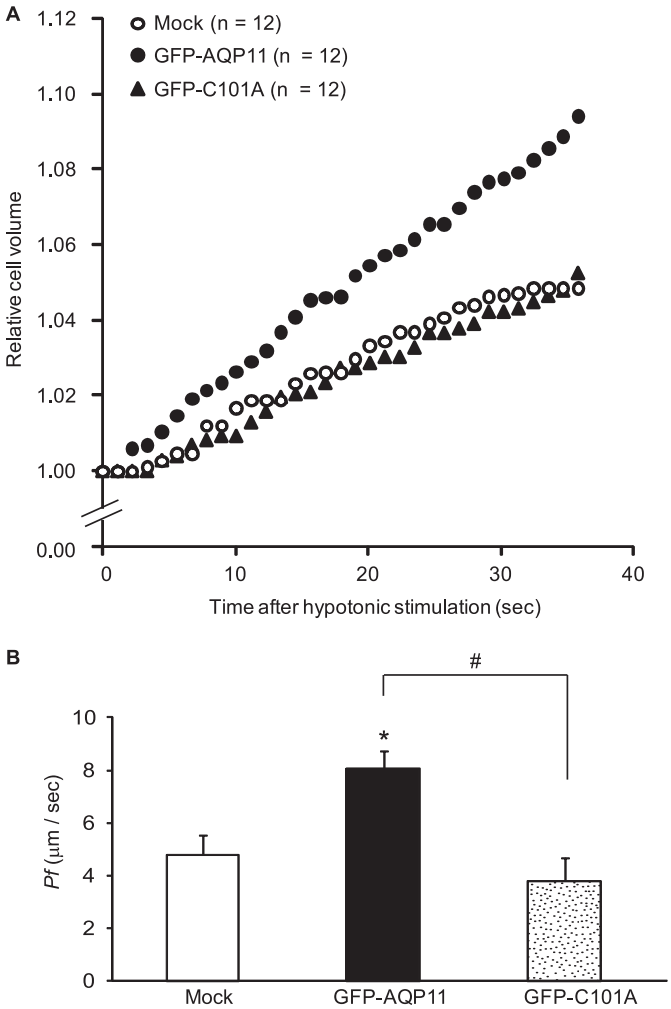

FIGURE 5. **Osmotic water permeability of cells expressing wild-type AQP11 or AQP11-C101A.** *A*, CHO cells were transfected with GFP-AQP11 or GFP-AQP11-C101A (*GFP-C101A*) expression plasmid. In the mock group, cells received the same reagent treatment to transfect but without adding the plasmid. After 24 h, the cell diameter was measured under a microscope. At time 0, the cells were exposed to hypotonic solution (300 to 150 mosmol solution). An image frame of the cell was recorded every 1.12 s with the microscope equipped with a time lapse image capture system. Values are presented as the mean. The numbers of cells tested are given in *parentheses*. *B*, *Pf* values were calculated from osmotic swelling data from *A* between 1.12 and 15.68 s using the formula as indicated (Equation 1). Values are presented as mean ± S.E. (*error bars*). *, $p < 0.05$ *versus* mock. #, $p < 0.01$ *versus* GFP-AQP11-C101A. Statistical significance was evaluated by Dunnett's test.

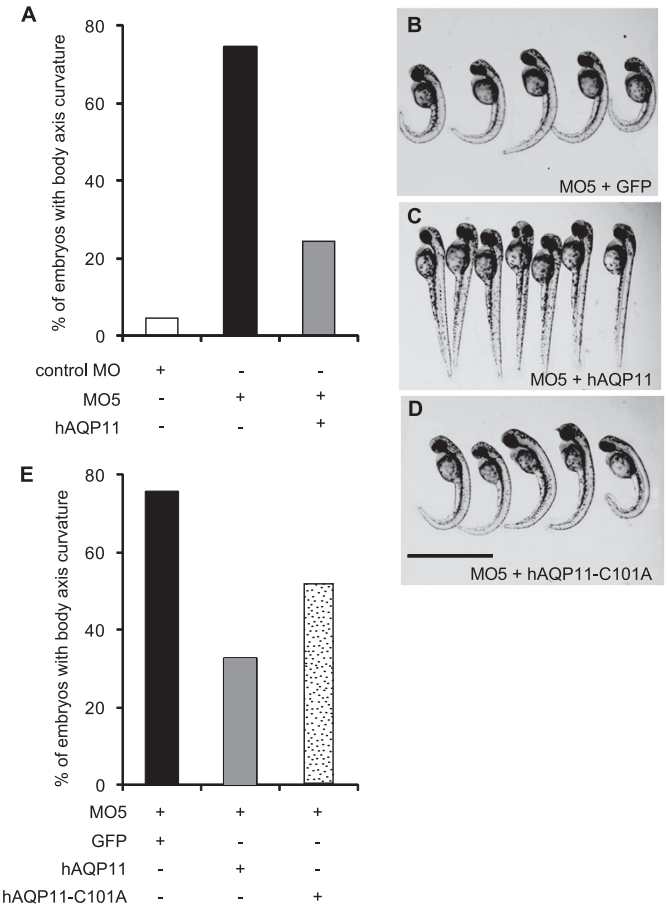

FIGURE 6. **The effect of capped hAQP11 or hAQP11-C101A mRNA on body axis curvature of endogenous AQP11-deficient morphants.** *A*, *bar graph* showing the percentage of larvae with body axis curvature, when a control MO, MO5, or MO5 + capped human AQP11 mRNA (hAQP11) was injected into one-cell-stage embryos. For each experimental condition, more than 48 embryos were injected. *B–D*, examples of body shape of 48-h postfertilization zebrafish larvae are shown, when MO5 + capped GFP mRNA (*GFP*) (*B*), MO5 + hAQP11 (*C*), or MO5 + capped human AQP11-C101A mRNA (*hAQP11-C101A*) (*D*) was injected into one-cell-stage embryos. *Scale bar*, 2 mm. *E*, *bar graph* showing the percentage of larvae with body axis curvature, when MO5 + GFP, MO5 + hAQP11, or MO5 + hAQP11-C101A was injected into one-cell-stage embryos. For each experimental condition, more than 60 embryos were injected.

We injected MO5 into one-cell-stage embryos and macroscopically observed the phenotype at days 1–5 after injection. Fig. 6*A* summarizes the data in the same batches of morphants at 2 days after injection. When the control MO (5-bp mismatched MO5) was injected into the embryos, only 4.5% of the morphants exhibited body axis curvature. In contrast, more than 70% of morphants with MO5 did so. However, this malformation was observed in only 24% of morphants that had received a co-injection of both MO5 and hAQP11 cap RNA. Similar results were obtained at the other time points studied. These data are in good agreement with the previous observations and suggest that the functions of human and zebrafish AQP11 are interchangeable.

Using this technique, we next examined the effect of hAQP11-C101A cap RNA on the MO5-induced phenotype. In Fig. 6, *B–D* show representative photographs, *E* summarizes the data from the same batches of morphants at 2 days after injection. When MO5 and GFP cap RNA (as a control cap RNA) were co-administered, 76% of the morphants showed body axis curvature. The frequency of occurrence of the abnormal phenotype was reduced when we used hAQP11 instead of GFP cap RNA. After co-administration of hAQP11-C101A with MO5, 52% of the morphants showed body axis curvature, suggesting that the AQP11-C101A mutant had reduced ability to rescue the malformation induced by MO5 compared with that of the wild-type AQP11.

DISCUSSION

Both water-selective AQPs and aquaglyceroporins are known to have two highly conserved NPA motifs that represent the signature motifs of the AQP family (1, 2). The third AQP group is the subgroup that has been proposed most recently (2, 5), and it is characterized by the divergence of an

N-terminal NPA motif with conservation of the C-terminal NPA motif. As yet, the function of the third AQP group has been little characterized, and the role of the divergent NPA motif has not been elucidated. AQP11 belongs to this group with an N-terminal NPC motif, and the present study attempted to clarify the role of this motif. Fluorescence microscopy and biotinylation experiments indicated that the NPC motif played no significant role in the subcellular localization of AQP11. Co-immunoprecipitation and cross-linking studies showed that the NPC motif was important for the multimerization of AQP11, and a cell swelling assay revealed that the motif was necessary for AQP11 water permeability. Furthermore, experiments with zebrafish showed that the functions of human and zebrafish AQP11 were exchangeable and that introduction of mutation in the NPC motif lowered the function of AQP11. Based on these data, we conclude that the N-terminal NPC motif of AQP11 is essential for full functionality of the molecule. Moreover, our observations seem to highlight the functional importance of the divergent N-terminal motif for members of the third AQP group.

The water-selective AQPs characterized to date form tetramers, and each monomer contains a channel (2). Many biochemical and structural studies have demonstrated that water-selective AQPs have a high degree of similarity in their amino acid sequences and that their monomers have the same topological characteristics (2). The topological model includes six transmembrane domains (TM1 to -6) connected to each other by five loops (A–E) with two conserved NPA motifs in loops B and E. In this study, co-immunoprecipitation and cross-linking experiments demonstrated that the unique NPC motif of AQP11, corresponding to the N-terminal NPA motif of the water-selective AQPs, plays an important role in its three-dimensional protein structure. According to the three-dimensional models, the quaternary structure of AQP1 is stabilized by interaction between TM1 and TM5 of the neighboring monomer as well as between TM2 and TM4 of the neighboring monomer. Furthermore the N- and C-terminal domains of AQP1 are thought to be involved in its tetramer formation (2–4, 20, 21). Recently, it has also been reported that although the residues are unique to AQP1, Lys^{51} of TM2 interacts with Asp^{185} of TM5 on an adjacent monomer to stabilize the AQP1 tetramer (22). Because the degree of amino acid sequence similarity between AQP11 and other AQPs is rather low, it is difficult to predict the three-dimensional structure of AQP11 using homology modeling (7). However, if the quaternary structure of AQP11 is similar to those of known AQPs, and Cys^{101} of AQP11 is located in loop B, then the residue may not be positioned in the domains that are considered important for the multimerization of AQP1 through direct interaction with other monomers. Therefore, mutation at Cys^{101} of AQP11 may interfere with formation of the correct structure within the individual subunit, leading to misalignment of surrounding contact points between subunits. In fact, when we preliminarily built three-dimensional structure models of both AQP11 and AQP11-C101A using the AQP1 crystal structure as a template, the mutation at Cys^{101} caused a misalignment in a C-terminal domain after TM5 (especially at the junction between loop E and TM6) of AQP11. Future crystallographic studies will be necessary to assess more definitively the structure of the AQP11 oligomer.

Numerous theoretical analyses have shown that the water-selective AQPs have two narrow constrictions (2, 3). The narrowest constriction is located close to the extracellular pore mouth, which consists of Arg in an aromatic environment. The second, less narrow, constriction is located at the center of the pore, and this constriction is formed by the two Asn residues in two NPA motifs. The two Asn residues are thought to act as hydrogen donors to the oxygen atoms of passing permeants. According to this model, two NPA motifs are essential for transfer of water molecules through the water-selective AQPs. In the present study, we examined the effect of mutation in the N-terminal NPC motif on the water permeability of AQP11. Although the effect of the C101A mutation on multimerization was partial, the mutation almost abolished the water permeability of AQP11. Again, if the three-dimensional structure of AQP11 is assumed to resemble those of known AQPs, the Cys^{101} is positioned at a site at or near the second constriction region. Therefore, it is likely that the mutation at Cys^{101} may change the structure around the second constriction region, leading to a greater effect on water permeation than on multimerization.

The present study clearly demonstrated the water permeability of AQP11, in good agreement with previously reported data (12), indicating that AQP11 is a water channel protein. In view of its water permeability, AQP11 is thought to be similar to the water-selective AQPs. However, our data indicated the importance of the NPC motif for the full functionality of AQP11, whereas the corresponding NPA motif was a signature motif for the water-selective AQPs (1, 2, 5), suggesting that AQP11 is a protein distinct from the water-selective AQPs. Furthermore, the amino acid sequence alignments show that Cys at the ninth residue downstream of the C-terminal NPA motif is well conserved in the members that are thought to belong to the third AQP group, whereas this Cys is not conserved in either the water-selective AQPs or the aquaglyceroporins (5). Recently, a point mutation of Ser at this Cys of AQP11 was reported to produce a phenotype similar to that of AQP11-null mice (9), suggesting that Cys^{227} is important for the function of AQP11. Therefore, AQP11 should be preferably placed in a new class of the AQP subfamily, the third AQP group, in which deviation of the N-terminal NPA motif and Cys at the ninth residue downstream of the C-terminal NPA motif may be a defining characteristic.

In contrast to the mutational effect on water permeability, our zebrafish experiments showed that mutation at Cys^{101} of the NPC motif did not result in complete loss of function. Because the zebrafish lives in waters at temperatures below the culture temperature for transfected mammalian cells, the differential effect of the mutation between the water permeability and zebrafish phenotype may result from a temperature-dependent effect of the mutant. We therefore preliminarily measured the osmotic water permeabilities of cells expressing AQP11 and AQP11-C101A as well as the mock cells at a temperature (15 °C) lower than that (25 °C) used in Fig. 5. The *Pf* values, shown as mean ± S.E., were $2.8 \pm 0.6 \times 10^{-4}$ cm/s ($n = 6$) for cells expressing AQP11, $2.9 \pm 0.7 \times$

10^{-4} cm/s ($n = 6$) for AQP11-C101A, and $3.8 \pm 0.6 \times 10^{-4}$ cm/s ($n = 6$) for the mock cells, and there was no significant difference between the three groups. These results strongly suggest that the differential effect of the mutation between the water permeability and zebrafish phenotype does not result from a temperature-dependent effect of the mutant. On the other hand, a partial effect of the mutation was also observed in the oligomerization study, suggesting that the full function of hAQP11 in zebrafish appears to be related to the correct tertiary and/or quaternary structure rather than to water permeation. Besides functioning as channels for water and small solutes, some evidence indicates that AQPs play a structural role involved in cell-to-cell adhesion. Electron crystallography and atomic force microscopy studies have shown that AQP0, a lens-specific AQP molecule, formed single layered as well as double layered crystals, suggesting that AQP0 has an adhesive role in the ocular lens fibers (23, 24). High resolution structures of AQP0 have also shown the interaction with lipid (25). Because mutations of AQP0 have been observed in patients with cataract (26–28), this adhesion is thought to be involved in the maintenance of lens transparency. Similarly to AQP0, it has also been reported that each AQP4 tetramer interacts with four tetramers in the opposing membrane (29). Although the pathophysiological significance of this structure of AQP4 is still not clear (30), it is suggested that the structure mediates AQP4-dependent adhesion. We do not know whether this is the case for AQP11, but it is considered that the correct tertiary and/or quaternary structure of AQP11 is necessary for a structural role of the molecule inside or/and outside cells and that this role may be important for the function of hAQP11 in zebrafish.

It has been reported that loss of function of AQP11 in mice causes polycystic kidney disease (6, 9). We also checked the kidney development in morphants with MO5. However, renal cyst formation was not observed (data not shown). Recently, a profile of AQP gene expression in zebrafish was reported (19). In that study, RT-PCR analysis clearly showed a lack of expression of the zebrafish *aqp11* gene (*draqp11b*) in the kidney. These findings together with our results indicate that AQP11 plays no significant role in kidney development in the zebrafish, suggesting differences in the role of AQP11 between species. Because the gene structure of zebrafish *aqp11* has not been completely established (19), the presence of alternatively spliced forms of AQP11 is possible. Future studies will be required to clarify the role of AQP11 in zebrafish.

In this study, injection of MO5 clearly caused a deformity in the tail region of the zebrafish. Because a number of genes are suggested to be involved in the body axis curvature of zebrafish (31) and the roles of AQPs in the body shape development of teleosts are unknown (32), it is difficult to discuss how AQP11 deficiency in zebrafish might induce body shape mutants with a curled tail. However, several recent studies seem to have hinted at the mechanisms underlying the body axis curvature induced by deficiency of AQP11 in zebrafish. Using microarray analyses, Okada *et al.* (33) have shown that the kidneys of 1-week-old AQP11-null and wild-type mice exhibit a significant change in the expression of three genes (*Myc*, *Egfr*, and *Egf*) involved in cell proliferation and three genes associated with remodeling of the extracellular matrix (*Mmp12*, *Timp1*, and *Tgfb1*). Expression of *Myc*, *Egfr*, *Mmp12*, *Timp1*, and *Tgfb1* was found to be up-regulated in $Aqp11^{-/-}$ mice, whereas *Egf* was down-regulated. So far, both enhancement of TGF-β1 signaling (34) and inhibition of EGF-signaling (35) have been reported to inhibit hormone-induced maturation of zebrafish oocytes. Therefore, it is considered that knockdown of zebrafish AQP11 by MO5 causes up-regulation of *Tgfb1* and down-regulation of *Egf*, thereby inhibiting the normal development of zebrafish and leading to curvature of the body axis. Array analysis to characterize the gene expression profile in zebrafish with AQP11 deficiency is now in progress in our laboratory.

The present study has provided a novel approach employing paraformaldehyde for studying the native quaternary structure of AQP11, and using this simple method, we succeeded in detecting oligomeric forms of AQP11, as shown in Fig. 2. This was in good agreement with the results obtained using paraformaldehyde for detecting multimeric forms of membrane proteins, such as synaptophysin, vesicle-associated membrane protein II, secretory carrier membrane protein, and 25-kDa synaptosome-associated protein (17). Formaldehyde has been used as a fixative for a long time, but the precise mechanism whereby it cross-links protein has not been fully understood. However, it has been shown that the protein-protein cross-links induced by paraformaldehyde can be as short as one carbon atom and that the predominant cross-link species seem to be the methylene bridge (17). A methylene bridge connecting the nitrogen atoms of two Lys side chains is estimated to be ~3 Å long. For comparison, the cross-link distance obtained with the commonly used homobifunctional *N*-hydroxysuccinimide ester cross-linker DSP would be 12.0 Å (data from the Pierce catalogue). The successful use of paraformaldehyde for cross-linking in this study appears to be an indication that the narrowest distance between each monomer of AQP11 is around 3 Å in an AQP11 oligomer. In order to define this clearly, a combination of paraformaldehyde cross-linking and crystallography will be required.

In summary, the present results indicate that a unique NPC motif of AQP11 corresponding to the NPA motif found in conventional AQPs has an important role in the function of the molecule. Similarly to AQP11, AQP12 is thought to belong to the third group of AQPs because it also has a divergent N-terminal NPA motif (8). Furthermore, other AQPs with a divergent N-terminal NPA motif, which could also be members of this group, have been reported in nematodes, fruit fly, fish, frog, and chicken (5). We anticipate that the results of the present study will help to clarify the function of members of the third AQP group at the molecular level.

REFERENCES

1. Carbrey, J. M., and Agre, P. (2009) *Handb. Exp. Pharmacol.* **190,** 3–28
2. Walz, T., Fujiyoshi, Y., and Engel, A. (2009) *Handb. Exp. Pharmacol.* **190,** 31–56
3. Murata, K., Mitsuoka, K., Hirai, T., Walz, T., Agre, P., Heymann, J. B., Engel, A., and Fujiyoshi, Y. (2000) *Nature* **407,** 599–605
4. Mathai, J. C., and Agre, P. (1999) *Biochemistry* **38,** 923–928
5. Ishibashi, K., Koike, S., Kondo, S., Hara, S., and Tanaka, Y. (2009) *J. Med.*

Invest. **56,** (suppl.) 312–317
6. Morishita, Y., Matsuzaki, T., Hara-chikuma, M., Andoo, A., Shimono, M., Matsuki, A., Kobayashi, K., Ikeda, M., Yamamoto, T., Verkman, A., Kusano, E., Ookawara, S., Takata, K., Sasaki, S., and Ishibashi, K. (2005) *Mol. Cell Biol.* **25,** 7770–7779
7. Gorelick, D. A., Praetorius, J., Tsunenari, T., Nielsen, S., and Agre, P. (2006) *BMC Biochem.* **7,** 14
8. Itoh, T., Rai, T., Kuwahara, M., Ko, S. B., Uchida, S., Sasaki, S., and Ishibashi, K. (2005) *Biochem. Biophys. Res. Commun.* **330,** 832–838
9. Tchekneva, E. E., Khuchua, Z., Davis, L. S., Kadkina, V., Dunn, S. R., Bachman, S., Ishibashi, K., Rinchik, E. M., Harris, R. C., Dikov, M. M., and Breyer, M. D. (2008) *J. Am. Soc. Nephrol.* **19,** 1955–1964
10. Yeung, C. H., and Cooper, T. G. (2010) *Reproduction* **139,** 209–216
11. Larsen, H. S., Ruus, A. K., Schreurs, O., and Galtung, H. K. (2010) *Eur. J. Oral Sci.* **118,** 9–13
12. Yakata, K., Hiroaki, Y., Ishibashi, K., Sohara, E., Sasaki, S., Mitsuoka, K., and Fujiyoshi, Y. (2007) *Biochim. Biophys. Acta* **1768,** 688–693
13. Ikeda, M., Beitz, E., Kozono, D., Guggino, W. B., Agre, P., and Yasui, M. (2002) *J. Biol. Chem.* **277,** 39873–39879
14. Ikeda, M., Fong, P., Cheng, J., Boletta, A., Qian, F., Zhang, X. M., Cai, H., Germino, G. G., and Guggino, W. B. (2006) *Cell Physiol. Biochem.* **18,** 9–20
15. Uechi, T., Nakajima, Y., Chakraborty, A., Torihara, H., Higa, S., and Kenmochi, N. (2008) *Hum. Mol. Genet.* **17,** 3204–3211
16. Neely, J. D., Christensen, B. M., Nielsen, S., and Agre, P. (1999) *Biochemistry* **38,** 11156–11163
17. Hannah, M. J., Weiss, U., and Huttner, W. B. (1998) *Methods* **16,** 170–181
18. Morrical, S. O., Kane, M. E., DeChant, B. T., Ishibashi, K., and Obara, M. (2006) *J. Am. Soc. Nephrol.* **17,** (suppl.) 538A–539A
19. Tingaud-Sequeira, A., Calusinska, M., Finn, R. N., Chauvigné, F., Lozano, J., and Cerdà, J. (2010) *BMC Evol. Biol.* **10,** 38
20. Jung, J. S., Preston, G. M., Smith, B. L., Guggino, W. B., and Agre, P. (1994) *J. Biol. Chem.* **269,** 14648–14654
21. Duchesne, L., Pellerin, I., Delamarche, C., Deschamps, S., Lagree, V., Froger, A., Bonnec, G., Thomas, D., and Hubert, J. F. (2002) *J. Biol. Chem.* **277,** 20598–20604
22. Buck, T. M., Wagner, J., Grund, S., and Skach, W. R. (2007) *Nat. Struct. Mol. Biol.* **14,** 762–769
23. Hasler, L., Walz, T., Tittmann, P., Gross, H., Kistler, J., and Engel, A. (1998) *J. Mol. Biol.* **279,** 855–864
24. Fotiadis, D., Hasler, L., Müller, D. J., Stahlberg, H., Kistler, J., and Engel, A. (2000) *J. Mol. Biol.* **300,** 779–789
25. Gonen, T., Cheng, Y., Sliz, P., Hiroaki, Y., Fujiyoshi, Y., Harrison, S. C., and Walz, T. (2005) *Nature* **438,** 633–638
26. Berry, V., Francis, P., Kaushal, S., Moore, A., and Bhattacharya, S. (2000) *Nat. Genet.* **25,** 15–17
27. Geyer, D. D., Spence, M. A., Johannes, M., Flodman, P., Clancy, K. P., Berry, R., Sparkes, R. S., Jonsen, M. D., Isenberg, S. J., and Bateman, J. B. (2006) *Am. J. Ophthalmol.* **141,** 761–763
28. Gu, F., Zhai, H., Li, D., Zhao, L., Li, C., Huang, S., and Ma, X. (2007) *Mol. Vis.* **13,** 1651–1656
29. Hiroaki, Y., Tani, K., Kamegawa, A., Gyobu, N., Nishikawa, K., Suzuki, H., Walz, T., Sasaki, S., Mitsuoka, K., Kimura, K., Mizoguchi, A., and Fujiyoshi, Y. (2006) *J. Mol. Biol.* **355,** 628–639
30. Verkman, A. S. (2009) *J. Exp. Biol.* **212,** 1707–1715
31. Brand, M., Heisenberg, C. P., Warga, R. M., Pelegri, F., Karlstrom, R. O., Beuchle, D., Picker, A., Jiang, Y. J., Furutani-Seiki, M., van Eeden, F. J., Granato, M., Haffter, P., Hammerschmidt, M., Kane, D. A., Kelsh, R. N., Mullins, M. C., Odenthal, J., and Nüsslein-Volhard, C. (1996) *Development* **123,** 129–142
32. Cerdà, J., and Finn, R. N. (2010) *J. Exp. Zool. A Ecol. Genet. Physiol.* **313,** 623–650
33. Okada, S., Misaka, T., Tanaka, Y., Matsumoto, I., Ishibashi, K., Sasaki, S., and Abe, K. (2008) *FASEB J.* **22,** 3672–3684
34. Kohli, G., Hu, S., Clelland, E., Di Muccio, T., Rothenstein, J., and Peng, C. (2003) *Endocrinology* **144,** 1931–1941
35. Pang, Y., and Ge, W. (2002) *Endocrinology* **143,** 47–54